JOURNAL OF THE ACOUSTICAL SOCIETY

OF THE REPUBLIC OF CHINA

December 1996 Vol.4, No.1

CONTENTS

PAPER

SHORT PAPER

Journal of The Acoistical Society of R.O.C., Vol.4 No.1 pp.39-61 (1996)

The Evaluation of Cost Functions for Active Sound Radiation Control of a Simply-Supported Beam

Bor-Tsuen Wang

Department of Mechanical Engineering

National Pingtung Polytechnic Institute

Pngtung, Taiwan 91207

Republic of China

ABSTRACT

This paper provides a general idea for selecting cost functions regarding to the availability of sensing techniques. A simply-supported beam with infinite rigid baffle subject to harmonic point force is considered. The PZT actuator is applied as control inputs in conjunction with the adoption of LMS feedforward control algorithm. Either accelerometers, microphones or strip PVDF film sensors can be used as error sensors. Ideal sensors such as vibrating energy, radiated acoustic power and supersonic wavenumber transform components are also considered. In particular, the discrete Fourier wavenumber transorm (DFWT) approach with the use of a series of accelerometers or PVDF film sensors is also presented and compared. Ten types of cost functions are defined and to be minimized in order to perform sound radiation control. Control mechanisms are shown through the radiation directivity patterns and wavenumber analysis for an on-resonance excitation case. A wide range of different excitatiion frequencies is also presented to show their control effectiveness. This work provides a systematic approach for selecting the cost function regarding to the different sensing approaches for active sound radiation control of the beam. The control characteristics of different cost functions are also shown.

簡支樑之主動聲音輻射控制之成本函數評估

王栢村

國立屏東技術學院機械工程技術系

摘　要

本文基於現有感測技術提供選用成本函數之分析，考慮一具有無長剛體屏障之簡支樑受一簡諧點力作用，應用最小平方前饋控制方式，以壓電驅動器爲控制源，分別以加速度計、麥克風或壓電膜爲感應器，也考慮理想式感應器，如振動能量、聲音輻射能量或超音波波數，以及以一系列之加速度計或壓電薄膜感應器，取其傅立葉波數轉換以作波數模式感應，本文共定義十種成本函數配合作結構聲音輻射控制，針對共振激振爲例，分別以聲音輻射指向圖及波數域分析，探討其控制特性，並對不同之激振頻率以比較其控制效果，本文基於不同之感測技術，提供一系統性選擇成本函數之分析，應用於樑聲音輻射之主動控制，並評估不同成本函數之控制效果，將來亦可應用至其它結構系統。

Introduction

The selection of cost functions is very important and generally determines the effectiveness of sound radiation control. The definition of cost function is usually dependent on the types of error sensor used in the control system. Discrete types of sensors such as microphones [1-4], accelerometers [5-7] and PVDF films [8-11] can be used as the error sensors for structural sound radiation control. Their performance for a beam sound radiatiion control is studied by Wang [12]. Microphones are conventionally used and shown effective; however, that microphones were located in the far-fiield sometimes makes them impractical. Accelerometers and PVDF films are structural sensors which can only provide structural dynamic response instead of acoustic response. Since the structural sound radiation is strongly correlated to the structural dynamic response, such structural sensors can be sufficient for sound radiation control. Either a strip [13] or a shaped [14] PVDF film sensor is also shown effective for structural sound radiation control. Distributed types of ideal sensors such as vibrating energy or radiated sound power can also be formulated to perform sound radiation control; however, they can not be measured directly. Model reference control [15,16] can be applied to implement such an ideal cost function. Alternately, as many as accelerometer distributed over the structure or microphones distributed over the hemisphere of radiated sound field can be used to obtain the approximate vibrating energy [17,18] or radiated sound power [19,20]. However, the discretization error is inevitable, and the approximation may not be well enough to represent the actual system response.

Wavenumber domain approach is firstly proposed by Fuller and Burdisso [21]. They constructed the cost function as the mean square value of the supersonic wavenumber components corresponding to a prescribed microphone position. The control can be effectively achieved by minimizing the cost function. Sommerfeldt [22] developed an ideal wavenumber domain control approach. He included all of the supersonic wavenumber components as the cost function, i.e., the radiated sound power equivalently. Maillard and Fuller [23,24] used several accelerometers as the error sensors by performing the discrete Fourier wavenumber transorm (DFWT) for wavenumber sensing to construct the cost function associated with a prescriged radiation angle. Wang [25] developed the PVDF based wavenumber domain sensing techniques for sound radiation control of simply-supported beam. A series of PVDF films are equally spaced and distributed over the beam length. With the use of the DFWT approach, the wavenumber transfer functions (WTFs) can be obtained such that the cost function can be defined.

This paper considers the simply-supported beam with infinite rigid baffle subject to

a harmonic point force excitation, while the PZT actuator is used as the control input. Based upon the availability of sensing approach, the systematic approach of selecting cost function is presentd. Ten types of cost functions associated with practical or ideal sensing approaches are defined. Either one of the cost function is shown quadratic and definite-positive and possesses a unique minimum. The linear quadratic optimal control theory (LQOCT) [26] can then be applied to determine the optimal inputs to the control actuators so as to numerically simulate the LMS feedforward control algorithm. Numerical simulations are shown to physically study the control mechanisms for each type of cost function. Without the consideration of optimal placement of actuators and sensors, the control performance are compared. The cases of different excitation frequencies over a wide range are also shown to evaluate the performance of cost functions.

2.THEORETICAL ANALYSIS

2.1 Lateral Vibration of Uniform Beam

Consider a uniform simply-supported beam with length of L, as shown in Figure 1. The beam lateral displacement $w\ (x,t)$ due to harmonic excitation can be expressed as follows:

$$w(x,t) = e^{jwt} \sum_{n-1}^{\infty} q_n(\omega)\phi_n(x) \tag{1}$$

where

$$\phi(x) = \sin \alpha_n x \tag{2}$$

$$\alpha_n = \frac{n\pi}{L} \tag{3}$$

The modal amplitudes $q_n(\omega)$ depend on the form of excitation force. For a harmonic point force F applying at x_f, the modal amplitude can be shown as

$$q_n^f(\omega) = H_n(\omega)\phi_n^f(x_f)F \tag{4}$$

where

$$\omega_n = \alpha_n^2 \sqrt{\frac{E_b I}{\rho_b b t_b}} \tag{5}$$

$$\phi_n^f(x_f) = \sin \alpha_n x_f \tag{6}$$

$$H_n(\omega) = \frac{1}{\rho_b b t_b (\omega_n^2 - \omega^2)} \tag{7}$$

It is noted that $\phi_n^f(x_f)$ is the displacement mode shape of the beam at coordinate x_f. for an actuator consisting of two identical piezoceramic patches bonded symmetrically on

the two opposite beam surfaces and activated 180° out-of-phase, the corresponding modal amplitude can be derived as follows:

$$q_n^c(\omega) = H_n(\omega)\phi_n^c(x_c)M_{eq} \tag{8}$$

where

$$\phi_n^c(x_c) = \phi_n'(x_1) - \phi_n'(x_2) = 2\alpha_n \sin(\alpha_n l_c/2)\phi_n(x_c) \tag{9}$$

It is noted that $\phi_n^c(x_c)$ is the slope difference mode shape between the two edges of the PZT actuator at coordinates x_1, x_2 and can be expressed by the displacement mode shape of the beam at the central location of the PZT patch, x_c, for simply-supported beam. For a PVDF film arranged as shown in Figure 1, the generated voltage can be shown as

$$V(x,t) = e^{j\omega t}K_p \sum_{n=1}^{\infty} q_n(\omega)\phi_n^p(x_p) \tag{10}$$

where

$$\phi_n^p(x_p) = \phi_n'(x_{p1}) - \phi_n'(x_{p2}) = 2\alpha_n \sin(\alpha_n l_p/2)\phi_n(x_p) \tag{11}$$

$$K_p = \frac{t_p}{\epsilon A}\frac{t_b + t_p}{2}e_{31}b_p \tag{12}$$

It is noted that the generated voltage is proportional to the slope difference between the two edges of a PVDF film.

2.2 Sound radiation from the beam

The far-field radiated sound pressure from the beam due to the point force and PZT actuator can be derived from Rayleigh integral and shown respectively [27]:

$$p_f(r,\theta,\phi,t) = e^{j\omega t}\sum_{n=1}^{\infty} H_n(\omega)\phi_n^f(x_f)Fg_n(r,\theta,\phi) \tag{13}$$

$$p_c(r,\theta,\phi,t) = e^{j\omega t}\sum_{n=1}^{\infty} H_n(\omega)\phi_n^c(x_c)M_{eq}g_n(r,\theta,\phi) \tag{14}$$

where

$$g_n(r,\theta,\phi) = -j\omega\frac{\rho c b}{\pi}\frac{\kappa}{\alpha_n}\frac{e^{-j\kappa r}}{2r}\left[\frac{1-(-1)^n e^{-j\alpha}}{1-(\alpha/n\pi)^2}\right]\left[\frac{1-e^{-j\beta}}{\beta}\right] \tag{15}$$

$$\alpha = \kappa L \sin\theta\cos\phi \tag{16}$$

$$\beta = \kappa b \sin\theta \sin\phi \tag{17}$$

Under the assumption of superposition, the total radiated sound pressure can be the sum of sound pressures due to the disturbance and control inputs

$$p_t = p_f + p_c = e^{i\omega t}\sum_{n=1}^{\infty}[\phi_n^f(x)F + \phi_n^c(x_c)M_{eq}]H_n(\omega)g_n(r,\theta,\phi) \tag{18}$$

The total radiated sound power defined as the integral of the square of the radiated sound pressure over the hemisphere of the radiating field can then be obtained:

$$\Phi_p = \frac{1}{2\rho c}\int_s |p_t|^2 dS = \frac{r^2}{2\rho c}\int_0^{2\pi}\int_0^{\pi/2} |p_t|^2 \sin\theta d\theta d\phi \tag{19}$$

The total radiated sound power can be an index to evaluate the effectiveness of sound radiation control.

2.3 Wavenumber Analysis

The beam acceleration can be taken Fourier wavenumber transform in κ-plane and shown as follows by neglecting the harmonic time function.

$$\tilde{V}_w = (\kappa_x,\ \kappa_y) = \int_{-\infty}^{\infty}\int_{-\infty}^{\infty}\ddot{w}(x,y)e^{-j(\kappa_x x+\kappa_y y)}dxdy \tag{20}$$

where

$$\kappa_x = \kappa\sin\theta\cos\phi \tag{21}$$

$$\kappa_y = \kappa\sin\theta\sin\phi \tag{22}$$

For one-dimensional beam application, the y-direction response is negligible; therefore, the beam acceleration wavenumber transform function (WTF) by performing continuous Fourier wavenumber transform (CFWT) neglecting the time component can be expressed as:

$$\tilde{V}_w(\kappa_x,\ \kappa_y) = -\omega^2[\frac{e^{-j\kappa_y b}-1}{-j\kappa_y}]\sum_{n=1}^{\infty}q_n(\omega)\tilde{\phi}_n(\kappa_x) \tag{23}$$

where

$$\tilde{\phi}_n(\kappa_x) = \int_{-\infty}^{\infty}\phi_n(x)e^{-j\kappa_x x}dx = \int_0^L \phi_n(x)e^{-j\kappa_x x}dx = \alpha_n[\frac{1-(-1)^n e^{-j\kappa_x L}}{\alpha_n^2-\kappa_x^2}] \tag{24}$$

$\tilde{\phi}_n(\kappa_x)$ is the continuous Fourier wavenumber transform of $\phi_n(x)$ and can be approximated by discrete Fourier wavenumber transform (DFWT)

$$\tilde{\phi}_n(m \triangle \kappa_x) = \sum_{i=1}^{N} \phi_n(i \triangle x) e^{-j(\frac{mi}{N})} \triangle x, \qquad m = 0, 1, 2, ..., N-1 \tag{25}$$

where

$$\triangle \kappa_x = \frac{1}{L} \tag{26}$$

$$N = \frac{L}{\triangle x} \tag{27}$$

N is the number of discretization, i.e., the number sensor applied in practical measurement; and $\triangle x$ is the equal distance apart between sensors. The acceleration WTF by performing DFWT for $\kappa_y = 0$ can then be derived:

$$\tilde{V}_{w-DFT}(m \triangle \kappa_x) = jb\omega^2 \sum_{n=1}^{\infty} q_n(\omega) \sum_{i=1}^{N} \phi_n(i \triangle x) e^{-j(\frac{mi}{N})} \triangle x, \qquad m = 0, 1, 2, ..., N-1 \tag{28}$$

Similarly, the generated voltages from the PVDF film shown in Eq. (10) can also be taken CFWT in κ-plane and derived as follows:

$$\tilde{V}_V(\kappa_x, \kappa_y) = K_p[\frac{e^{-j\kappa_y b} - 1}{-j\kappa_y}] \sum_{n=1}^{\infty} q_n(\omega) \tilde{\phi}_n^p(\kappa_x) \tag{29}$$

where

$$\tilde{\phi}_n^p(\kappa_x) = \int_0^L \phi_n^p(x) e^{-j\kappa_x x} dx = 2\alpha_n^2 \sin(\alpha_n l_p/2)[\frac{1 - (-1)^n e^{-j\kappa_x L}}{\alpha_n^2 - \kappa_x^2}] \tag{30}$$

Again, the continuous Fourier wavenumber transform can be approximated by the discrete Fourier wavenumber transform; therefore, the PVDF voltage WTF by performing the DFWT for $\kappa_y = 0$ can be obtained

$$\tilde{V}_{V-DFT}(m \triangle \kappa_x) = -jb \sum_{n=1}^{\infty} q_n(\omega) \tilde{\phi}_n^p(m \triangle \kappa_x), \qquad m = 0, 1, 2, ..., N-1 \tag{31}$$

where

$$\tilde{\phi}_n^p(m \triangle \kappa_x) = \sum_{i=1}^{N} \phi_n^p(i \triangle x) e^{-j(\frac{mi}{N})} \triangle x, \qquad m = 0, 1, 2, ..., N-1 \tag{32}$$

$\tilde{\phi}_n(m \triangle \kappa_x)$ denotes the m-th wavenumber components of the PVDF mode shape $\phi_n^p(x)$ by performing discrete Fourier wavenumber transform; and $i \triangle x$ is the spatial coordinate of the i-th sensor location.

2.4 Cost Functions

For vibration control, the most general cost function can be formed as the integral of the mean squared beam lateral acceleration over the beam. Such a cost function gives a global sense of vibration level attenuation (in particular, it is proportional to the total vibrational energy density); however, in practical application, it is difficult to measure a distributed acceleration. Instead, a finite number of accelerometers can be imposed to the beam to measure the accelerations. The objective here is to apply an minimization procedure for a quadratic function developed by Lester and Fuller [2] using tensor calculus, and to calculate the input amplitude of the control source such that a selected cost function can be minimized. The derivation of the minimization process for the uniform beam applying distributed or discrete sensors was shown previously [28].

For sound radiation control, microphones located in the far-field are generally used as error sensors; however, near-field structural sensors are preferred for easy implementation. The PVDF film, a distributed type of sensor, is recently applied to measure the structural response and acts as a near-field structural sensor to perform active sound radiation control. Also, the radiated sound power can be ideally constructed as the cost function to perform active control. Therefore, different types of cost functions can be constructed as follow. The LQOCT can then be applied to obtain the optimal control voltage to the piezoelectric actuator so as to minimize the cost function.

1. Discrete Acceleration Sensor

For the use of N_a accelerometers, the cost function can be defined as the sum of the mean square of measured accelerations:

$$\Psi_w = \sum_{j=1}^{N_a} |\ddot{w}(x_{aj})|^2 \tag{33}$$

2. Distributed Acceleration Sensor

The cost function corresponding to the distributed acceleration sensor can be defined as follows:

$$\Phi_w = \int_0^L |\ddot{w}_t|^2 dx \tag{34}$$

It is noted that Φ_w can be viewed as the out-of-plane vibration energy density which can used as an index to evaluate the effectiveness of vibration control.

3. Distributed PVDF Film Sensor

For the use of N_s PVDF film sensors, the cost function can be defined as the sum of

the mean square voltages measured from the PVDF films:

$$\Psi_v = \sum_{j=1}^{N_s} |V_j|^2 \tag{35}$$

4. Discrete Pressure Sensor

For the use of N_m microphones, the cost function can be defined as the sum of the mean square of measured sound pressure:

$$\Psi_p = \sum_{j=1}^{N_m} |p_t(r_j, \theta_j, \phi_j)|^2 \tag{36}$$

5. Distributed Pressure Sensor

The cost function corresponding to the distributed pressure sensor can be defined as the total radiated power as shown previously:

$$\Phi_p = \frac{1}{2\rho c} \int_s |p_t|^2 ds \tag{37}$$

It is noted that the radiated power can be used as an index to evaluate the effectiveness of sound radiation control.

6. Discrete Wavenumber Sensor

The cost function can be defined as the sum of the mean square of the prescribed supersonic wavenumber components corresponding to the use of N_m micrlophones:

$$\Psi_k = \sum_{j=1}^{N_m} |\tilde{V}_w(\kappa_{xj} = \kappa \sin\theta_j \cos\phi_j)| \tag{38}$$

As discussed, only the supersonic wavenumber components will radiate into the far-field; therefore, it is reasonable to specify the supersonic wavenumber component as the cost function. Each wavenumber component can be associated with a radiation angle which can be considered as the location of microphone.

7. Wavenumber sensing approach based on distributed accelerometer sensor

It is noted that the mean square value of the acceleration wavenumber transform, i.e., $|\tilde{V}_w|^2$, integrated over the supersonic region is proportional to the radiated sound power [29]. Only the wavenumber components satisfying $\kappa_x^2 + \kappa_y^2 < \kappa^2$ contribute to sound radiation into the far-field and are termed as supersonic waves. The remaining wavenumber components

associated with the subsonic waves do not radiate into the far-field. Therefore, it is reasonable to construct the cost function based on the acceleration wavenumber transform functions as follows:

$$\Phi_{k,w} = \int_{-\kappa}^{\kappa} |\tilde{V}_w(\kappa_x, \kappa_y = 0)|^2 d\kappa_x \tag{39}$$

8. Wavenumber sensing approach based on distributed PVDF sensor

Similar to Eq. (39), the cost function based on the PVDF voltages wavenumber transform functions can be defined as follows:

$$\Phi_{k,V} = \int_{-\kappa}^{\kappa} |\tilde{V}_V(\kappa_x, \kappa_y = 0)|^2 d\kappa_x \tag{40}$$

9. Wavenumber sensing approach based on collocated accelerometer sensors

It is noted that $\Phi_{k,w}$ is the integration of supersonic wavenumber components which contribute the sound radiation into far-field. $\Phi_{k,w}$ is also known proportional to the radiated sound power. Therefore, choosing $\Phi_{k,w}$ as the cost function is similar to choosing the radiated sound power as the cost function. $\Phi_{k,V}$ is the integration of PVDF voltage wavenumber transform functions in the supersonic region. By examining Equations (23) and (29), $\Phi_{k,V}$ can be somewhat related to radiated sound power, and so forth it is reasonable to select $\Phi_{k,V}$ as the cost function. Both $\Phi_{k,w}$ and $\Phi_{k,V}$ are continuous functions obtained from acceleration and PVDF voltage wavenumber transform functions based on the CFWT approach. It is noted that these two cost functions can not be measured directly in reality, although these cost functions are highly correlated to the structural sound radiation. With the use of a series of accelerometers or strip PVDF film sensors in conjunction with the DFWT approach, the discrete wavenumber transform functions based on accelerometers and PVDF sensors can be obtained through Equations (23) and (29). Notice that only positive wavenumber components can be obtained, and only the components below the Nyquist wavenumber $\kappa_{x,Nyq} = \frac{N}{2}\kappa_x$ are valid. Analogy to the Eq. (39) for the CFWT approach, the cost function based on the DFWT approach for accelerometers can be defined

$$\Phi_{k,w-DFT} = \sum_{m=0}^{N_\kappa} |\tilde{V}_{w-DFT}(m \triangle \kappa_x)|^2, \qquad N_\kappa = \frac{\kappa}{\triangle \kappa_x} + 1 \tag{41}$$

10. Wavenumber sensing approach based on collocated PVDF sensors

Analogy to the Eq. (40) for the CFWT approach, the cost function based on the DFWT approach for PVDF sensors can be defined

$$\Phi_{k,V-DFT} = \sum_{m=0}^{N_\kappa} |\tilde{V}_{V-DFT}(m \triangle \kappa_x)|^2, \qquad N_\kappa = \frac{\kappa}{\triangle \kappa_x} + 1 \tag{42}$$

$\Phi_{k,w-DFT}$ and $\Phi_{k,V-DFT}$ represent the sum of mean square value of the positive supersonic wavenumber components of the acceleration and PVDF voltage WTFs respectively; and N_κ is the minumum number of wavenumber component such that $N_\kappa = \frac{\kappa}{\triangle \kappa_x} + 1$. It is noted that $\Phi_{k,w-DFT}$ and $\Phi_{k,V-DFT}$ can be measurable and can be used to approximate the cost functions $\Phi_{k,w}$ and $\Phi_{k,V}$. In summary, $\Phi_{k,w}$ and $\Phi_{k,V}$ derived from the CFWT approach are ideal cost functions which are not measurable. $\Phi_{k,w-DFT}$ and $\Phi_{k,V-DFT}$ are defined from the acceleration and PVDF voltage WTFs by the DFWT approach and can be obtained by using a series of equally spaced accelerometers and PVDF sensors respectively. Although ideal sensing approaches, such as Φ_w, Φ_p, $\Phi_{k,w}$ and $\Phi_{k,V}$ are not practically measurable, the model reference control algorithm [16] can be applied to adopt any one of the ideal cost functions as the reference signal, and therefore the control can be achieved and shown effective.

Either one of the cost functions mentioned above is obviously quadratic and positive definite and possesses a unique minumum. The linear quadratic potimal control theory (LQOCT) can then be applied to minimize the cost function so as to find the optimal control voltages input to the piezoelectric actuators. One can easily perform a minimization procedures [2] to calculate the optimal control parameters so as to minimize the cost function. The full analysis can be referred to [28] and omitted here for brevity.

3.NUMERICAL RESULTS AND DISCUSSIONS

A steel beam with length of 0.38m, width of 0.04m, and thickness of 2mm is used in the simulations. The first few natural frequencies are 33.2 Hz, 128.8Hz, 289.9Hz, 515.4Hz, 805.3Hz and 1159.6Hz. It is noted that no damping was included in the following analysis. The optimal process is suitable for controlling multiple primary sources; however, only one harmonic point force with input parameters, F=0.3N and x_f=0.067m, was considered for the following analysis. The piezoceramic patch (G-1195) [30] and PVDF films (LDT-28μk) [31] are respectively used. The piezoceramic patch is located at x_1=0.285m, x_2=0.3485m. For discrete types of sensors, the accelerometer is assumed to be located at x_a=0.095m; the PVDF film at x_{p1}=0.075m, x_{p2}=0.105m; the microphone at (r, θ, ϕ)=(3m,-45°, 0°). The radial distance from the beam is assumed to be 3m, which was well into far-field. For wavenumber sensing approach, a series of strip PVDF films are spatially distributed over the beam length as shown in Figure 1(b). The strip PVDF film is assumed to be 0.02m length. For the

purpose of comparison, a series of accelerometers are also used and assumed to be located at the central location of PVDF films so as to perform the wavenumber sensing approach. In order to study the controllability of the wavenumber sensing approach, the cost function derived from the CFWT approach shown in Equations (39) and (40) are also numerically simulated. An on-resonance excitation case of f =290Hz near the third resonance is shown to demonstrate the sound radiation control effectiveness. Both accelerometers and PVDF sensors are respectively used, and the CFWT and DFWT approaches are also compared. Both the radiation directivity and WTF distributions were shown to demonstrate the control mechanism of the wavenumber sensing approach. The radiated sound pressure is calculated at a radial distance of 3m from the beam and plotted in dB re 20×10^{-6} Pa over $\theta = -90^o$ to 90^o for ϕ=0^o. In order to calculate the beam response and radiated sound pressure, it was necessary to truncate the modal sums in Equation (1). Upon the consideration of computing time and accuracy, the first 10 modes were considered, and it was found to provide sufficient convergence of the series. Finally, the cases of different excitation frequencies up to 1000Hz are also simulated. The radiated sound power are plotted verse the excitation frequency for both before and after controlled.

Figure 2(a) shows the sound pressure level (SPL) distributions before and after controlled for the cases of Ψ_w, Φ_w, Ψ_v, Ψ_p and Φ_p for f=290Hz. The solid line represents the disturbance SPL distribution which is volumetric, and at θ=0^o is relativelyy larger which evidences the existence of the third resonance mode. One can see that SPL distributions are greatly reduced after controlled. In particular, for the case of Ψ_p a dip reveals at θ=-45^o which is right at the microphone position. For the case of Φ_p, the remaining SPL reveals a dipole response. It can be realized that the third modal response is well controlled and leaving the second modal response which is the less efficiently radiated mode. For either the case of Ψ_w, Φ_w or Ψ_v which actually use the vibration information to perform sound radiatiion control, the remaining SPL distribution shows the combination for first and second modal response. This can be postulated that the third vibration mode is well controlled; however, the radiation response is still dominated by the first and second modes.

Figure 2(b) shows the sound pressure level (SPL) distributions before and after controlled for the cases of Ψ_κ, $\Phi_{\kappa,w}$, $\Phi_{\kappa,V}$, $\Phi_{\kappa,w-DFT}$ (N=10) and $\Phi_{\kappa,V-DFT}$ (N=10) for f=290Hz. One can see that the SPL distributions are greatly reduced for all cases. For the case of Ψ_κ, a dip appears at θ=-45^o, ϕ=0^o. It is noted that Ψ_κ and Ψ_p are physically the same content and result in the same control characteristic, although Ψ_κ is for wavenumber component, while Ψ_p is for microphone sensors. Both the cases of $\Phi_{\kappa,w}$ and Φ_p have very similar results

because of their cost functions are physically the same, i.e., the radiated sound power, and integrated numerically. For the case of $\Phi_{\kappa,V}$ which uses the PVDF voltage WTF derived from the CFWT approach as the cost function, the remaining SPL distribution reveals the combination of the first and second modal responses. And, the case of $\Phi_{\kappa,V-DFT}$ results in the similar SPL distribuion to that of $\Phi_{\kappa,V}$ because both cost functions are physically the same content except that $\Phi_{\kappa,V}$ is based on the CFWT approach, and $\Phi_{\kappa,V-DFT}$ is based on the DFWT approach. It is interested to note that for $\Phi_{\kappa,V-DFT}$, a dip appears near θ=30^o which can be explained by the following wavenumber analysis.

Figures 3(a) and 3(b) show the acceleration WTF distributions corresponding to the cases of Figures 2(a) and 2(b). One can observe that the radiation directivity patterns can be the shape of acceleration WTF distributions in the supersonic region $-\kappa < \kappa_x < \kappa$. For example, the SPL distribution is shown like a monopole response for the disturbance in Figure 2, while the acceleration WTF distribution also reveals the monopole characteristic in the supersonic region. For vibrational sensing appraches, such as the cases of Ψ_w, Φ_w and Ψ_V, the remaining acceleration WTF distributions reveal a dipole characteristic in Figure 3(a); therefore, as shown in Figure 2(a) the remaining SPL distributions also evidence the existence of the second modal response. For the pressure sensors like Ψ_p and Φ_p, the dips are shown at κ_x=-3.756 for Ψ_p and κ_x=0 for Φ_p. The κ_x=-3.756 corresponds to the radiation angle θ=-45^o, ϕ=0^o which is right on the specified error microphone position. This explains the dip shown in Figure 2(a) for the case of Ψ_κ. For the case of Φ_p, the dip at κ=0 evidences that the dominant modal response of the third mode is well controlled and leaving the less efficiently radiated mode which is the second mode here. One should note that as discussed previously for the cases of Ψ_p and Ψ_κ and the cases of $\Phi_{\kappa,w}$ and Φ_p are physically identical; therefore, the remaining acceleration WTF distributions are also about the same. For the case of $\Phi_{\kappa,w-DFT}$, the remaining acceleration WTF has a dip near κ_x=2.631 which corresponding to the radiation angle θ=30°, Φ=0°. This can explain the dip at θ=30^o shown in Figure 2(b) for $\Phi_{\kappa,w-KFT}$ (N=10).

Table 1 shows the reduction of radiated sound power for different types of cost functions used in performing sound radiation control for f=290Hz. One can see that both the cases of Φ_p and $\Phi_{\kappa,w}$ can obtain the maximum reduction of radiation sound power about 62dB. The ideal sensors, such as Φ_w and $\Phi_{\kappa,V}$ can obtain about 57dB reduction of radiated sound power. As noted previously, these ideal sensors can not be practically measured. With the use of the discrete types of sensors, such as Ψ_w, Ψ_V and Ψ_p, the reductions of radiated sound power are 58, 53 and 26dB respectively. The structural sensors like the accelerometer and PVDF film

used here are located near the maximum response of the third structural mode; therefore, a large amount of reduction of radiated sound power can be obtained. The microphone is arbitrarily chosen to be located at θ=-45°, ϕ=0° at which position is not the optimal location; therefore, only 26dB can be obtained. Ψ_κ has the same amount of reduction of radiated sound power 26dB as that for Ψ_p, because both cost functions are physically the same content as noted before. For the cases of $\Phi_{\kappa,w-DFT}$ (N=10) and $\Phi_{\kappa,V-DFT}$ (N=10) which are the DFWT approximation for $\Phi_{\kappa,w}$ and $\Phi_{\kappa,V}$, the reduction of radiated sound power are 28dB and 46dB respectively. As expected, the control for the DFWT approach is not as well as that for the CFWT approach. In particular, the use of PVDF sensors is better than the use of accelerometers for f=290Hz.

To further examine the control performance for all of different types of cost functions at different excitation frequencies, the radiated sound powers before and after controlled verse excitation frequency are shown in Figures 4(a)-4(j). For the case of Ψ_w, since the accelerometer is located at 0.095m which is near the nodal point of the fourth structural mode, the sound radiation control become ineffective near the fourth resonance excitation. For other frequency excitation cases, control can be achieved except at some antiresonance points. It is noted that the PZT control actuator and accelerometer locations are not optimized. For the case of Ψ_w which is for the ideal vibration sensing approach, i.e., selecting vibrating energy as the cost function, the control can be effective except the antiresonance points. For the case of Ψ_V, the results are similar to that for Ψ_w, because both cost functions are almost identical for simply-supported beam application. For the cases of Φ_p and $\Phi_{\kappa,w}$, both cost functions can provide the best sound radiation control among all of the cost functions, because the cost functions are physically the same and represent the radiated sound power. Therefore, without considering the optimal placement of the actuators, the implementation of ideal pressure sensor and the acceleration wavenumber sensing approach can be the best. However, in reality, these ideal sensors may not be practically constructed. Some approaches can be performed to achieve the goals. First, the model reference control approach[15,16] can be applied to simulate the ideal distributed pressure or wavenumber sensing approach. Second, to use as many as error microphones at the hemisphere of the radiated sound field to approximately construct the radiated sound power. Third, a series of accelerometers or PVDF sensors can be applied as error sensors, and the DFWT approach can be performed in order to obtain the WTF such that the ideal distributed wavenumber components can be constructed. Figures 4(i) and 4(j) respectively show the results for $\Phi_{\kappa,w-DFT}$ (N=10) and $\Phi_{\kappa,V-DFT}$ (N=10). The control effectiveness is generally less than those of $\Phi_{\kappa,w}$ and $\Phi_{\kappa,V}$ for the CFWT approach; however, a certain amount of reduction of radiated sound power can

be obtained for on-resonance excitation. In particular, for the case of $\Phi_{\kappa,V-DFT}$ the control may not be effective for some cases of off-resonance excitation. Finally, for the cases of Ψ_p and Ψ_κ both cost functions are physically identical and result in quite similar results. Notice that only one microphone is used, i.e., only one wavenumber component corresponding to the radiation angle of the microphone is used, the control can be acheived; however, as expected the control performance is less effective than those of Φ_p and $\Psi_{\kappa,w}$.

In summary, the performance of Φ_p and $\Phi_{\kappa,w}$ are almost the same, and Ψ_p and Ψ_κ are the same too, because those cost functions are physically identical to each other. Φ_p and $\Phi_{\kappa,w}$ can provide the best control performance without the consideration of optimal placement of control actuators. The vibrational sensors, such as the cases of Ψ_w and Ψ_V, are physically measurable; however, the sensor's location may affect the control performance. As shown previously, the structural sensors should not be located near the nodal point of structural vibration mode. For ideal vibrational sensor, Φ_w, the control is effective and is not as well as the ideal pressure sensor Φ_p or the acceleration wavenumber sensing approach $\Phi_{\kappa,w}$. The DFWT approach can be performed with the use of a series of accelerometers or PVDF sensors to approximately obtain the WFTs so as to construct the appropriate cost functions which are based on the acceleration or PVDF voltage WFT and are correlated to the radiated sound power.

4. CONCLUSIONS

This paper numerically studies the control performance for various types of cost functions based on practical or ideal sensing approaches for sound radiation control of a simply-supported beam. Vibrational sensing devices such as accelerometers and PVDF films are considered. The ideal acceleration, pressure and wavenumber sensing approaches are also shown. A series of accelerometers or PVDF films with the use of the DFWT approach to construct the appropriate cost functions to approximate the ideal wavenumber sensing approaches are also compared. Without the consideration of optimal placement of control actuators or error sensors, the control mechanisms for ten types of cost functions associated with the different types of sensing techniques are studied. The results show that the ideal pressure or the acceleration wavenumber sensing approach which are not practically measurable can provide the best sound radiation control. Either model reference control approach, a number of error microphones to approximate the radiated sound power, or the DFWT approach with the use of a series of accelerometers or PVDF films can be used to achieve the sound radiation control. This work provides a systematic approach for selecting cost function

based on the use of error sensors in conjunction with the adoption of LMS feedforward control algorithms to actively control the sound radiation from a simply-supported beam. The ideas of selecting cost functions can be applied to other structural sound radiation control systems.

5. ACKNOWLEDGEMENTS

The author gratefully acknowledges the support of the work by National Science Council, Republic of China, under grant NSC84-2212-E-020-005.

6.REFEREMCES

1. Metcalf, V.L., Fuller, C.R., Silcox, R. J. and Brown, D. E. : Active Control of Sound Transmission/Radiation from Elastic Plates by Vibration Inputs-II Experiments. *J. Sound Vib.* 1992; 153:387-402.

2. Lester, H. C. and Fuller, C. R. : Active Control of Propeller Induced Noise Fields Inside a Flexible Cylinder. *AIAA J.* 1990; 28:1374-1380.

3. Deffayet, C. and Nelson, P. A. : Control of Low Frequency Harmonic Sound Radiated by a Finite Panel. *J. Acoust. Soc. Am.* 1988; 84:2192-2199.

4. Silcox, R. J., Lester, H. C. and Abler, S. B. : An Evaluation of Active Noise Control in a Cylindrical Shell. *J. Vib. Acoust. Stress Reliability Design* 1989; 111:337-342.

5. Fuller, C. R. and Jones, J. D. : Experiments on Reduction of Propeller Induced Interior Noise by Active Control of Cylinder viibration. *J. Sound Vib.* 1987; 112:389-395.

6. Pan, J., Snyder, S. D., Hansen, C. H. and Fuller, C. R. : Active Control of Far Field Sound Radiated by a Rectangular Panel - a General Analysis. *J. Acoust. Soc. Am.* 1992; 91:2056-2066.

7. Meirovitch, L., Baruh, H. and Oz, H. : A comparison of Control Techniques for Large Flexible Systems. *J. Guidance Control* 1983; 6:302-310.

8. Clark, R. L. and Fuller, C. R. : Control of Sound Radiation with Adaptive Structures. *J. Intell. Mat. Syst. Struct.* 1991; 2:431-452.

9. Clark, R. L. and Fuller, C. R. : Optimal Placement of Piezoelectric Actuators and Polyvinylidene Fluoride Error Sensors in Active Structural Acoustic Control Approaches. *J. Acoust. Soc. Am.* 1992; 92:1521-1533.

10. Clark, R. L., Burdisso, R. A. and Fuller, C. R. : Design Approaches for Shaping Polyvinyidene Fluoride Sensors in Active Structural Acoustic Control (ASAC). *J. Intell. Mat. Syst. Struct.* 1993; 4:354-365.

11. Wang, B. T. : Active Control of Far-Field Sound Radiation by a Beam with Piezoelectric Control Transducers : Physical System Analysis. *Smart Mater. Struct.* 1994; 3:476-484.

12. Wang, B. T. : The Performance of Accelerometers, Microphones and PVDF Sensors in Active Structural Acoustic Control : Theoretical Analysis. *Chinese J. of Mech.* 1994; 10:191-199.

13. Hubbard, J. E. : Distributed Sensors and Actuators for Vibration Control in Elastic Components. *Noise-Con 87* 1987; 407-412.

14. Lee, C. K. and Moon, F. C. : Modal Sensors/Actuators. *J. Appl. Mech.* 1990; 57:434-441.

15. Clark, R. L. and Fuller, C. R. : A Model Reference Approach for Implementing Active Structural Acoustic Control. *J. Acoust Soc. Am.* 1992; 92:1534-1544.

16. Clark, R. L., Gibbs, G. P. and Fuller, C. R. : Experimental Study Implementing Model Reference Active Structural Acoustic Control. *J. Acoust Soc. Am.* 1993; 93:3258-3264.

17. Pan, J. and Hansen, C. H. : Active Control of Total Vibratory Power Flow in a Beam, I: Physiical System Analysis. *J. Acoust Soc. Am.* 1990; 89:200-209.

18. Wang, B. T. and Fuller, C. R. : The Effect of Diistributed or Discrete Pressure and Acceleration Sensors on Active Structural Acoustic Control Systems. *J. Chinese Soc. Mech. Eng.* 1994; 15:30-39.

19. Naghshineh, K. : Active Control of Sound Power Using Acoustic Basis Functions as Surface Velocity Filters. *J. Acoust Soc. Am.* 1993; 93:2740-2752.

20. Elliott, S. J., Joseph, P., Nelson, P. A. and Johnson, M. E. : Power Output Minimization and Power Absorption in the Active Control of Sound. *J. Acoust Soc. Am.* 1991; 90:2501-2512.

21. Fuller, C. R. and Burdisso, R. A. : A Wavenumber Domain Approach to the Active Control of Structure-borne Sound. *J. Sound vib.* 1991; 148:355-360.

22. Sommerfeldt, S. : Active Wavenumber Control of Acoustic Radiatiion from a Plate. *Proceedings of the Second Conference on Recent Advances in Active Control of Sound and Vibration* 1993; 929-940.

23. Maillard, J. P. and Fuller, C. R. : Advanced Time Domain Wave-Number Sensing for Structural Acoustic Systems: I. Theory and Design. *J. Acoust. Soc. Am.* 1994; 95:3252-3261.

24. Maillard, J. P. and Fuller, C. R. : Advanced Time Domain Wave-Number Sensing for Structural Acoustic Systems: II. Active Radiation Control of a Simply Supported Beam. *J. Acoust. Soc. Am.* 1994; 95:3262-3272.

25. Wang, B. T. : *The Development of PVDF Based Wavenumber Domain Model Reference Sensiing Technique.* Republic of China, NSC Report: NSC84-2212-E-020-005, 1995.

26. Wang, B. T. : *Active Control of sound Transmission/Radiation From elastic Plates Using Multiple Piezoelectric Actuators.* Ph. D. Thesis, Department of Mechaniical Engineering, Virginia Polytechnic Institute and State Universiity, 1991.

27. Wallace, C. E. : Radiation Resistance of a Baffled Beam. *J. Acoust. Soc. Am.* 1972; 51:936-945.

28. Wang, B. T. : *A Dynamic Simulation of Hybrid Active and Passive Control of Structural Vibration*, Republic of China, NSC Report: NSC81-0401-E-020-501, 1992.

29. Fahy, F. : *Sound and Structural Vibration*, Orlando, Florida, Academic, 1985.

30. Piezo Systems, Inc. : *Product Catalog*, 1990.

31. Pennwalt Corporation, : *Piezo Film Sensor Application Notes*, 1990.

Appendix: List of Symbols

A	PVDF film area
b	beam width
b_p	PVDF width
c	air velocity
E_b	beam Young's modulus
e_{31}	piezoelectric strain constant of PVDF sensor
F	point force magnitude
$g_n(r,\theta,\phi)$	the n-th pressure modal amplitude
$H_n(\omega)$	the n-th mode transfer function
i	spatial sequence for the DFWT approach
I	moment inertia of the beam
K_p	some constant related to PVDF material properties
L	beam length
l_c	length of PZT actuator
l_p	length of PVDF sensor
M_{eq}	equivalent moment induced by PZT actuator
m	wavenumber sequence for the DFWT approach
N	number of spatial samples or number of sensors
N_κ	minimum number of wavenumber sequence such that $N_\kappa = \kappa/\triangle\kappa_x + 1$
$p_c,\ p_f,\ p_t$	sound pressure due to PZT excitation, point force and both
$q_n(\omega)$	the n-th modal amplitude
$q_n^c(\omega)$	the n-th modal amplitude due to PZT actuators
$q_n^f(\omega)$	the n-th modal amplitude due to point force (disturbance)
$r,\ \theta,\ \phi$	radiation field coordinates
t_b	beam thickness
t_p	PVDF thickness
$V(x,t)$	generated voltage from PVDF sensor
$\tilde{V}_V(\kappa_x,\ \kappa_y)$	PVDF voltage wavenumber transform function derived from the CFWT approach
$\tilde{V}_w(\kappa_x,\ \kappa_y)$	acceleration wavenumber transform function derived from the CFWT approach
$\tilde{V}_{V-DFT}(\kappa_x,\ \kappa_y)$	PVDF voltage wavenumber transform function derived from the DFWT approach
$\tilde{V}_{w-DFT}(\kappa_x,\ \kappa_y)$	acceleration wavenumber transform function derived from the DFWT approach
$w(x,t)$	beam lateral displacement
x_a	accelerometer actuator location
$x_c,\ x_1,\ x_2$	PZT actuator location
x_f	force location
$x_p,\ x_{p1},\ x_{p2}$	PVDF sensor location
α_n	normal mode wavenumber
$\triangle x$	equidistance of sensors
$\triangle\kappa_x$	wavenumber resolution

$\delta(x)$	Kronical delta function
ϵ	permittivity of PVDF film
$\Gamma(x)$	shape function of the PVDF sensor
κ	acoustic wavenumber
κ_x, κ_y	structural wavenumber
$\kappa_{x,Nyq}$	Nyquist wavenumber
ω	excitation frequency
ω_n	the n-th natural frequency
Φ_p	radiated sound power
$\Phi_{\kappa,V}$	cost function for PVDF based wavenumber sensing by the CFWT approach
$\Phi_{\kappa,w}$	cost function for accelerometer based wavenumber sensing by the CFWT approach
$\Phi_{\kappa,V-DFT}$	cost function for PVDF based wavenumber sensing by the DFWT approach
$\Phi_{\kappa,w-DFT}$	cost function for accelerometer based wavenumber sensing by the DFWT approach
$\phi_n(x)$	the n-th mode shape of the simply-supported beam
$\phi_n^c(x)$	the n-th PZT actuator mode shape of the simply-supported beam
$\phi_n^f(x)$	the n-th point force mode shape of the simply-supported beam
$\phi_n^p(x)$	the n-the PVDF sensor mode shape of the simply-supported beam
$\tilde{\phi}_n(\kappa_x)$	Fourier wavenumber transform of $\phi_n(x)$
$\tilde{\phi}_n^p(\kappa_x)$	Fourier wavenumber transform of $\phi_n^p(x)$
ρ	air density
ρ_b	beam density

Table 1. Results for the on-resonance excitation cases, f=290Hz

cost functiion	reduction of radiated sound power (dB)
Ψ_w	58.96
Φ_w	57.03
Ψ_V	53.94
Ψ_p	26.26
Φ_p	62.59
Ψ_κ	26.26
$\Phi_{\kappa,w}$	62.57
$\Phi_{\kappa,V}$	57.98
$\Phi_{\kappa,w-DFT}$(N=10)	28.79
$\Phi_{\kappa,V-DFT}$(N=10)	46.91

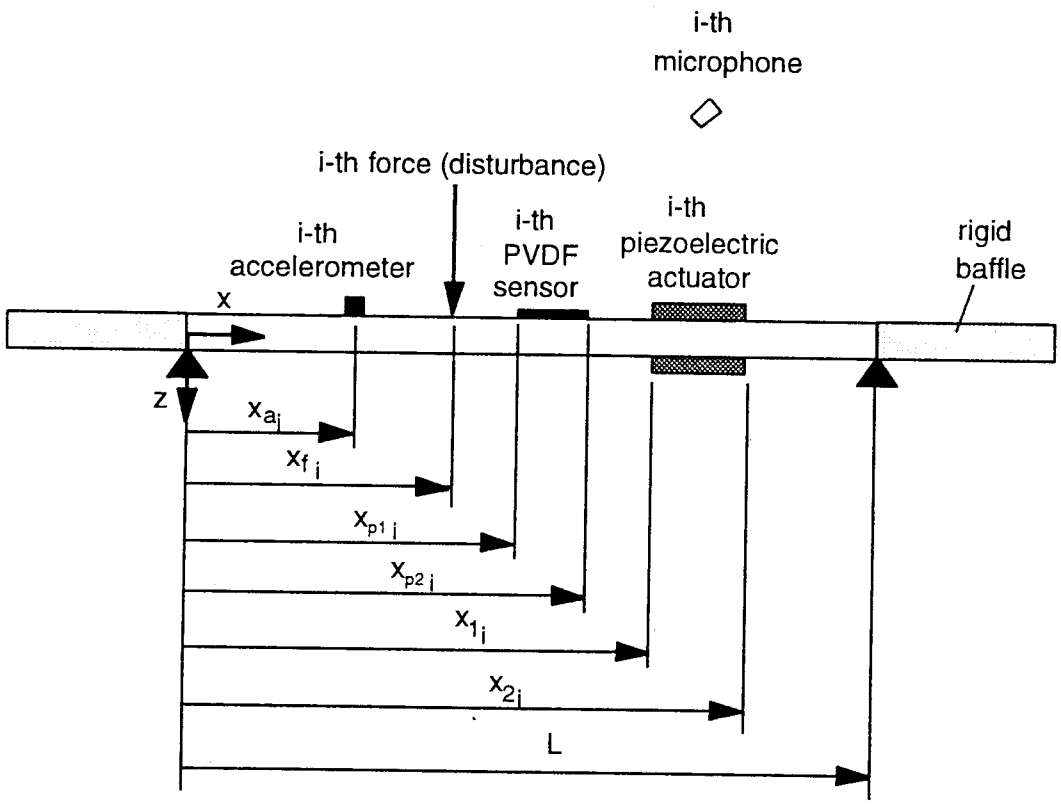

(a)

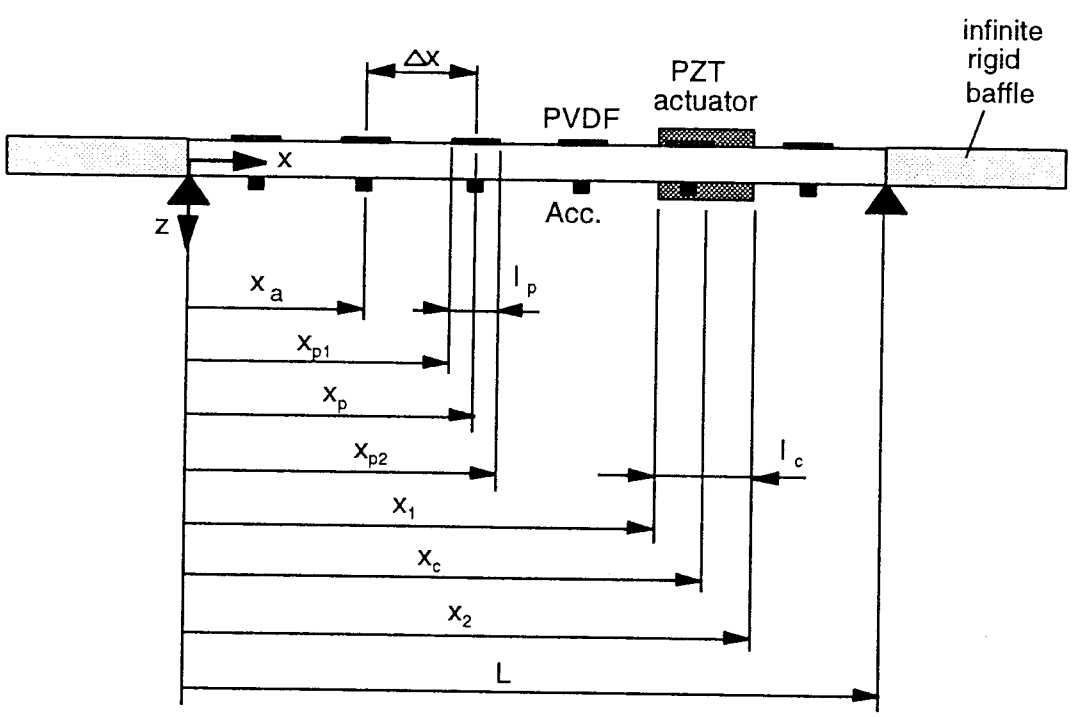

(b)

Figure 1. The arrangement and coordinates of simply-supported beam

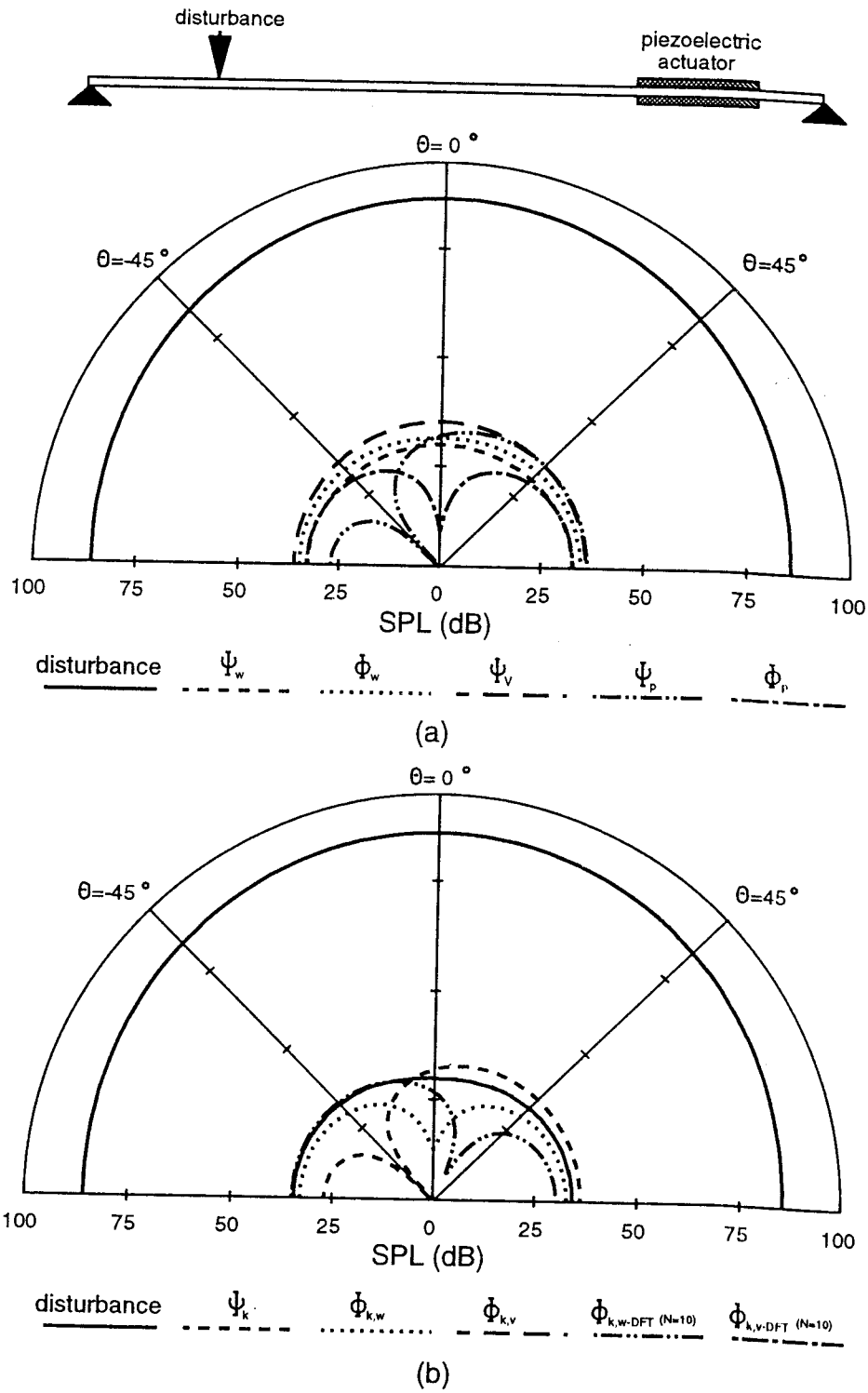

Figure 2. Sound pressure level distribution, f=290Hz

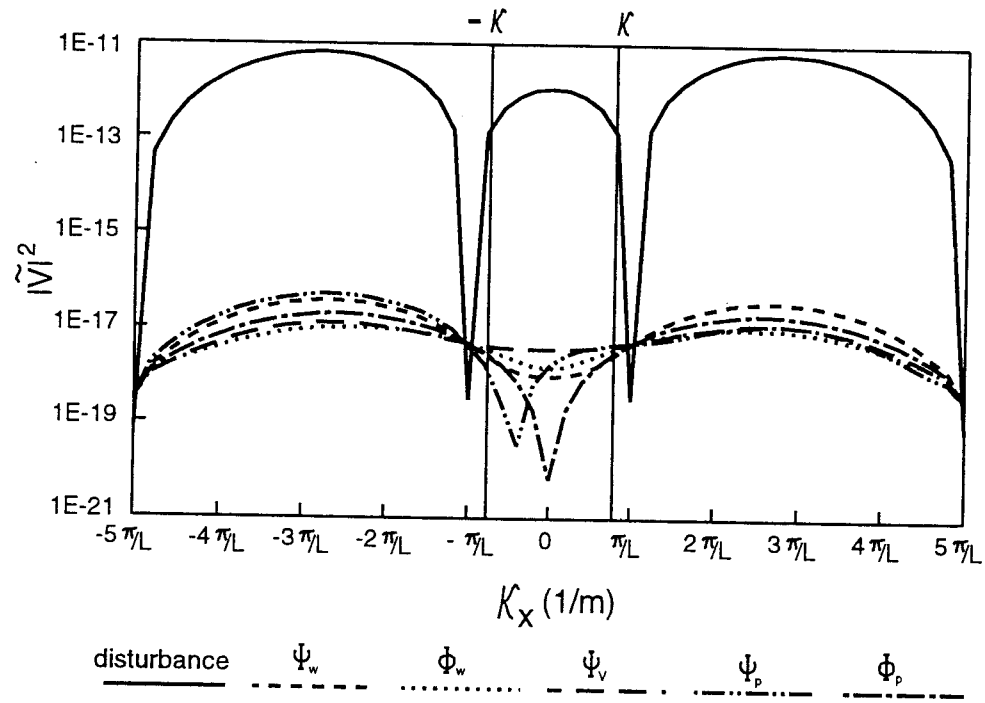

(a)

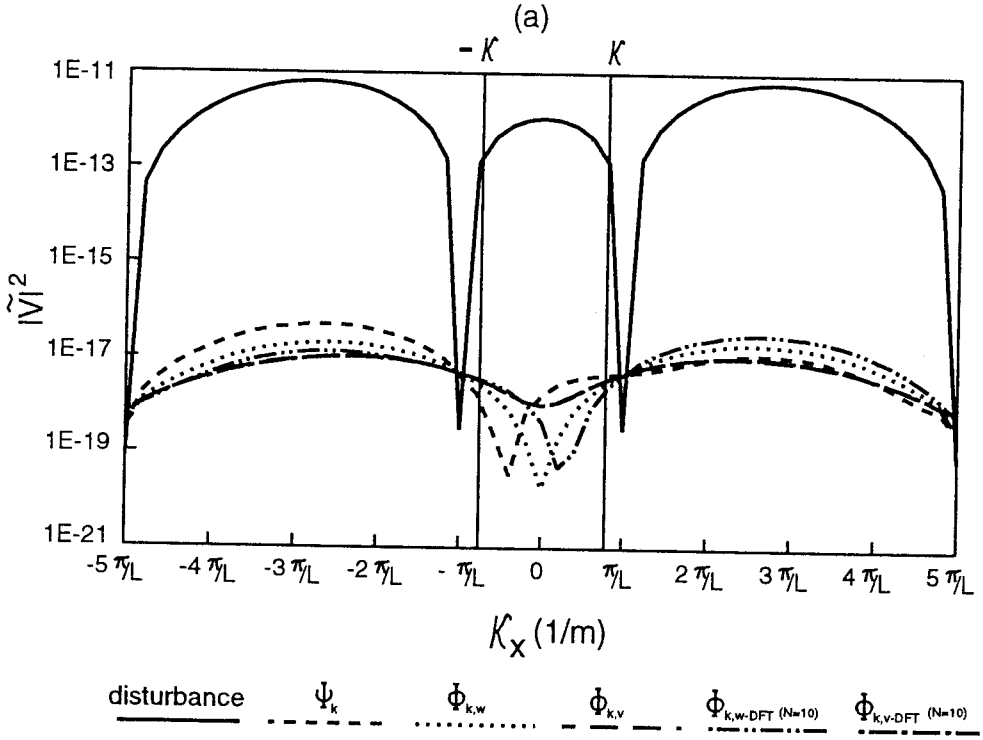

(b)

Figure 3. Acceleration WTF distribution, f=290Hz

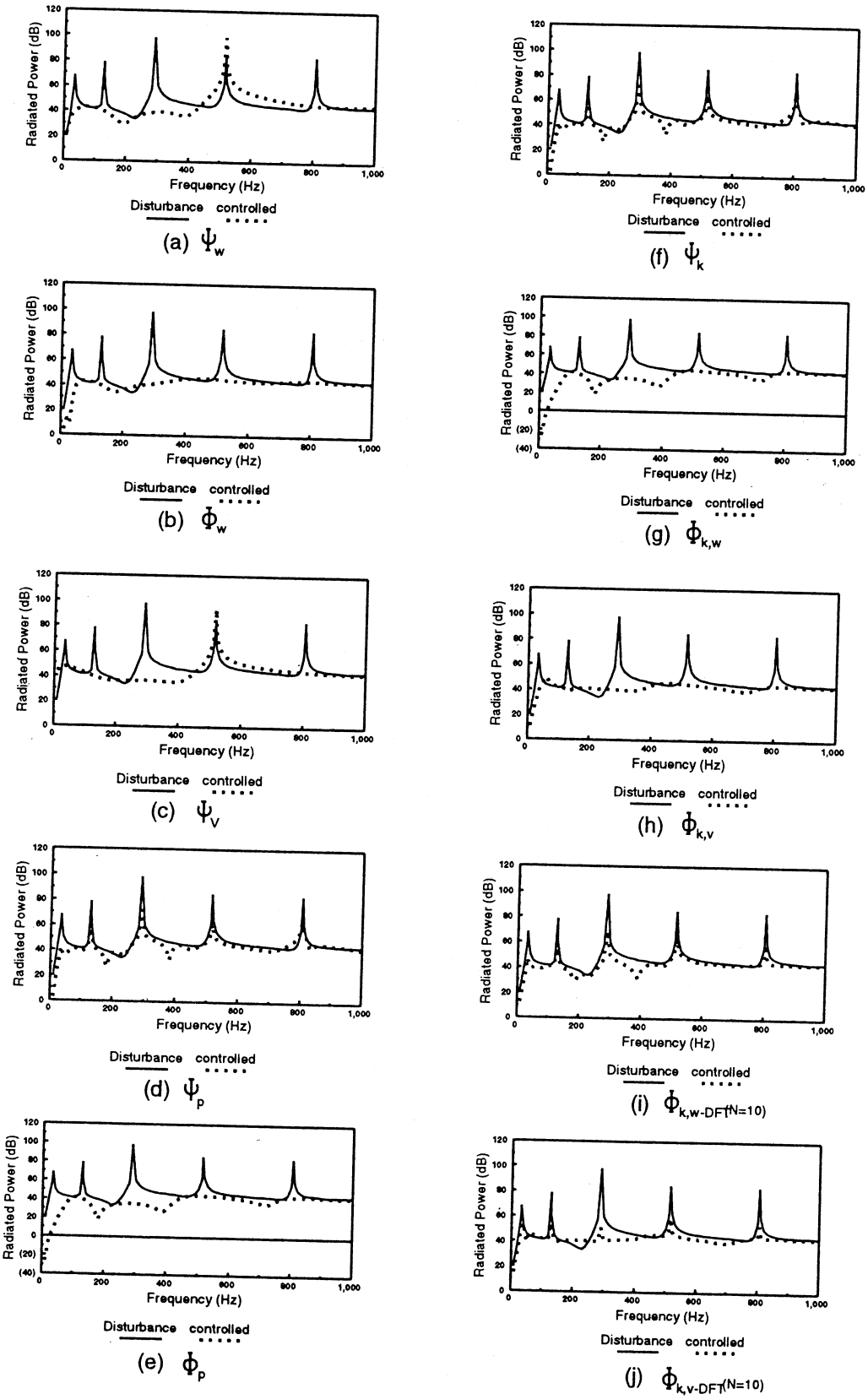

Figure 4. Radiated sound power vs. excitation frequency